Self-Synchronized Grid Impedance Estimation Unit using Interpolated DFT Technique

J. Mace, A. Cervone, and D. Dujic

Self-Synchronized Grid Impedance Estimation Unit using Interpolated DFT Technique

Jules Mace, *Student Member, IEEE,* Andrea Cervone, *Member, IEEE,* Drazen Dujic, *Senior Member, IEEE*

Abstract—Estimating the impedance of a grid-connected device or of a grid at the point of common coupling is important for evaluating the interaction between them. Impedance measurement involves a perturbation injection device, that perturbs the system, and a measurement device (impedance estimation unit) that acquires the grid voltages and currents to extract the impedance. When evaluating the grid impedance in the dq reference frame, the reference frame transformation requires estimating the grid angle. For a self-synchronized impedance estimation unit, angle estimation is typically performed by a phase-locked loop, but the presence of low-frequency voltage perturbations limits the accuracy of the results. This paper is proposing a method with a new approach, based on interpolated discrete Fourier transform technique, to extract the grid angle. Conventional phase locked loop and proposed interpolated discrete Fourier transform-based techniques are compared experimentally and the proposed technique shows more accurate impedance estimation in the low frequency range, for comparable frequency tracking performance.

Index Terms—Interpolated DFT, Grid Impedance Estimation, Phase Locked Loop, Perturbation Injection

I. INTRODUCTION

USE of power electronics converters in the grid for interfacing AC and DC grids [1], [2], renewable sources (wind turbine, PV source...) [3] or battery storage systems [4] is growing. However, the power conversion action of those controller-based actively regulating devices may result in instabilities and large harmonic power flows [5] in the grid as reported in several incidents that occurred in Switzerland in 1995 [6], in Germany in 2013 [7] and in France and Spain in 2016 [8], [9]. The origin of those faults is the interaction between the grid and the converters, and more precisely, between the grid impedance and the converter admittances that were not passive in the expected frequency range.

This impedance-admittance interaction, firstly investigated for DC/DC converters in the 1970s [10], has since then been expanded to the three-phase grid systems [11]–[13] and used for converter controller design and impedance/admittance measurements. While the converter impedance can be estimated using small-signal models of the converter [14], the grid impedance is typically unknown at the point of common coupling (PCC) in the grid, and therefore, must be extracted by experimental means. To obtain experimentally an impedance, a typical method is to inject a perturbation (voltage or current) and measure the voltages and currents, as response of the injected perturbations. The voltages and currents values over

All authors are with the Power Electronics Laboratory, Ecole Polytechnique Federale de Lausanne (EPFL), 1015 Lausanne, Switzerland, e-mail: jules.mace@epfl.ch, andrea.cervone@epfl.ch, drazen.dujic@epfl.ch
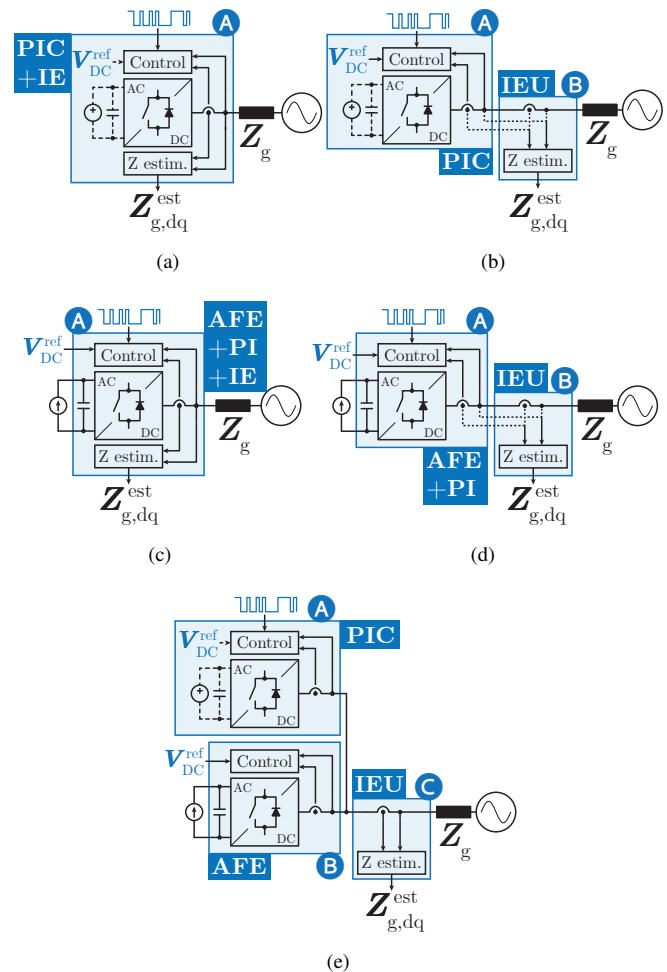
Fig. 1. Impedance estimation systems: perturbation injection converter (PIC) with (a) internal grid impedance estimation (IE) capability, (b) independent impedance estimation unit (IEU), (c)(d) power-processing converter (Active Front-End (AFE)) with perturbation injection (PI) capability, (e) power-processing converter, perturbation injection converter and independent impedance estimation unit.

the measurable frequency range are then extracted, allowing impedance computation in the frequency domain.

To perform the perturbation injection and the impedance extraction, several methods are possible using different sets of devices as sketched in Fig. 1. The perturbation source can either be generated by an ad-hoc converter with low power requirements (as in Figs. 1a, 1b and 1e) [15], [16] or be integrated in an existing grid-connected converter on top of its normal operation (as in Figs. 1c and 1d) [17], [18]. Similarly, the voltage/current measurements and the impedance estima-

tion can either be integrated with the perturbation injection converter (PIC) (Figs. 1a and 1c) [19] or be processed by an external Impedance Estimation Unit (IEU) (as in Figs. 1b, 1d and 1e) [16], [20].

Estimation of the impedance can be done in different reference frames: abc-frame [21]–[24], $\alpha\beta$ (stationary) reference frame or dq (synchronous) reference frame. In this last case, voltages and currents acquired are transformed in the dq-frame first, using an estimated grid angle, typically obtained with a phase-locked loop (PLL) computed by the PIC [15], [20], [25]–[27], or by one featured in the impedance measurement unit (IMU) [18], [28]. The PLL effect on the grid impedance computation has been extensively described in the literature [25], [28], [29]. Because the grid angle estimator (GAE) tracks the angle based on the voltages, perturbations on the grid voltages result in a distorted angle, impacting the grid impedance estimation, especially for low frequencies. A trade-off between a good grid angle tracking (large PLL bandwidth) and the quality of grid impedance estimation at low frequencies (small PLL bandwidth) must be found. The grid impedance at low frequencies is typically low (mainly comprised of the line resistance term) yet can still play a key role in the grid-converter interaction. It is therefore important to correctly estimate it.

On the other hand, extensive research has been conducted in the power system community to develop phasor measurement units (PMUs) with high speed acquisition systems, that can track the grid frequency with a very good precision. Interpolation-based method (interpolated discrete Fourier transform (IpDFT)) has for instance been developed to determine accurately the frequency between two DFT bins [30], [31]. PMU-based grid impedance measurement methods are also possible [32]–[36], but typically rely solely on grid voltage and current measurements, by extracting accurately the phasor at the fundamental frequency, without any perturbation being injected. Since the grid frequency is accurately estimated, by integrating it, it is consecutively possible to accurately estimate the grid angle, allowing for an impedance estimation in the dq reference frame. In the meantime, most of the research regarding grid impedance estimation relies on a grid angle estimated by real time devices [16], [20], [26] where those DFT techniques are not conventionally implemented because of their large computational burden. However, when the impedance is estimated in offline, so after the perturbation injection, the estimation is typically performed by computers with a high computational capacity (when compared to embedded devices's computational power) and the the objective is, in such applications, to reach high quality estimation. Proper angle estimation is then key for low frequency impedance estimation and the DFT-based approaches can be considered to improve the grid angle tracking.

This paper proposes a technique for an impedance extraction unit (IEU) that can extract impedances in the dq-frame based on PMU phasor estimation techniques. Since the grid angle estimation is performed internally, the impedance estimation unit is self-synchronizing. Compared to a conventional PLL-based method with an equivalent grid frequency tracking speed, the proposed IpDFT-based method can estimate the

grid impedance accurately for much lower frequencies, and the minimum frequency from which the impedance can be accurately estimated is clearly and simply defined.

This paper is structured as follows: in Section II, the effect of the grid angle estimation on the impedance estimation is introduced. In Section III, the proposed IpDFT-based method is presented. In Section IV, the experimental setup, including the perturbation injection converter and the impedance estimation unit, is described. In Section V, grid impedance is estimated using a state-of-the-art PLL method and the proposed IpDFT-based method as the grid angle estimator. Results are compared proving the proposed method to be a viable and convenient solution for grid impedance estimation in microgrids.

II. IMPACT OF THE GRID ANGLE ESTIMATION ON THE IMPEDANCE ESTIMATION

The impedance estimation in the dq frame is strictly linked to the knowledge of the fundamental grid angle. This is determined by a grid angle estimator that extracts the grid angle based on the grid voltages. The presence of perturbations (required for the impedance estimation) may alter the reliability of the results. This effect is here explained analytically.

Consider a grid voltages and currents perturbed by a small-signal perturbation:

$$\begin{cases} \boldsymbol{V}_{\mathrm{dq}}(t) = \boldsymbol{V}_{\mathrm{dq},0} + \boldsymbol{v}_{\mathrm{dq}}(t) \\ \boldsymbol{I}_{\mathrm{dq}}(t) = \boldsymbol{I}_{\mathrm{dq},0} + \boldsymbol{i}_{\mathrm{dq}}(t) \end{cases} \tag{1}$$

where $(\boldsymbol{V}_{\mathrm{dq},0}, \boldsymbol{I}_{\mathrm{dq},0})$ are the steady-state operating point and $(\boldsymbol{v}_{\mathrm{dq}}(t), \boldsymbol{i}_{\mathrm{dq}}(t))$ are the small-signal perturbations. Considering a grid angle estimator with the characteristic transfer function $G_{GAE}(s)$:

$$\Delta\theta_{\mathrm{g,p}}^{\mathrm{cap}}(s) = G_{\mathrm{GAE}}(s) \cdot \Delta\theta_{\mathrm{g,p}}(s) \tag{2}$$

where $\Delta\theta_{\mathrm{g,p}}^{\mathrm{cap}}(s)$ is the captured grid angle. It can be shown [25] that the grid angle estimator has an impact in the voltage and current estimation in the dq reference frame:

$$\begin{cases} \boldsymbol{V}_{\mathrm{dq}}^{\mathrm{est}}(s) &= \begin{bmatrix} 1 & 0 \\ 0 & 1 - G_{\mathrm{GAE}}(s) \end{bmatrix} \cdot \boldsymbol{V}_{\mathrm{dq}}(s) \\ \boldsymbol{I}_{\mathrm{dq}}^{\mathrm{est}}(s) &= \boldsymbol{I}_{\mathrm{dq}}(s) + \begin{bmatrix} 0 & \frac{I_{\mathrm{q},0}}{V_{\mathrm{d},0}} \cdot G_{\mathrm{GAE}}(s) \\ 0 & -\frac{I_{\mathrm{d},0}}{V_{\mathrm{d},0}} \cdot G_{\mathrm{GAE}}(s) \end{bmatrix} \cdot \boldsymbol{V}_{\mathrm{dq}}(s) \end{cases} \tag{3}$$

Hence, the computation of the grid impedance becomes:

$$\begin{aligned} \boldsymbol{Z}_{\mathrm{dq}}^{\mathrm{est}}(s) =& \boldsymbol{V}_{\mathrm{dq}}^{\mathrm{est}} \cdot \left(\boldsymbol{I}_{\mathrm{dq}}^{\mathrm{est}}\right)^{-1} \\ =& \begin{bmatrix} 1 & 0 \\ 0 & 1 - G_{\mathrm{GAE}}(s) \end{bmatrix} \\ & \cdot \left(\boldsymbol{Z}_{\mathrm{dq}}^{-1}(s) + \begin{bmatrix} 0 & \frac{I_{\mathrm{q},0}}{V_{\mathrm{d},0}} \cdot G_{\mathrm{GAE}}(s) \\ 0 & -\frac{I_{\mathrm{d},0}}{V_{\mathrm{d},0}} \cdot G_{\mathrm{GAE}}(s) \end{bmatrix} \right)^{-1} \end{aligned} \tag{4}$$

So, the estimation of $\boldsymbol{Z}_{\mathrm{dq}}$ is impacted by the response of the grid angle estimator, modeled by $G_{\mathrm{GAE}}(s)$. For an ideal grid impedance estimation, the grid angle estimator should have $G_{\mathrm{GAE}}(s) = 0$ for all frequencies, meaning that it

TABLE I
PLL CONTROLLER GAINS

Gain	Value
t_{set}	$100\,\text{ms}$
ξ	$\frac{1}{\sqrt{2}}$
ω_{n}	$\frac{1}{\xi\tau} = \frac{4.6}{\xi t_{\text{set}}} = 65\,\text{rad}\,\text{s}^{-1}$
$K_{\text{P,PLL}}$	$2\xi\omega_{\text{n}} = 92$
$K_{\text{I,PLL}}$	$\omega_{\text{n}}^2 = 4232$

Fig. 2. Bode plot of the PLL transfer functions G_{PLL} and $1 - G_{\text{PLL}}$ for the PLL gains of Table I.

should only track the fundamental components of the grid voltages, and completely disregard any perturbation. However, since the grid angle estimator must correctly track the slow grid frequency changes, the GAE transfer function must tend to 1 at low frequencies. Therefore, a trade-off between the transfer function tracking capability ($G_{\text{GAE}} \rightarrow 1$ at low frequencies) and good impedance estimation ($\boldsymbol{Z}_{\text{dq}}^{\text{est}} \rightarrow \boldsymbol{Z}_{\text{dq}}$ for all frequencies) must be found.

A. Conventional GAE: Phase-Locked Loop

The conventional methods [15], [25], [28] employed for GAE mostly use PLL to track the grid angle. The selected PLL gains are introduced in Table I, based on two parameters: the settling time t_{set} and the damping ratio ξ.

As presented in the previous section, the estimation of Z_{dq} is impacted by the response of the grid angle estimator, modeled by G_{GAE}. Using a simple PLL [37], $G_{\text{GAE}}(s)$ can be written as:

$$G_{\text{GAE}}(s) = G_{\text{PLL}}(s) = \frac{K_{\text{P}} \cdot s + K_{\text{I}}}{s^2 + K_{\text{P}} \cdot s + K_{\text{I}}} \quad (5)$$

The PLL response is a low-pass filter, hence, when used to estimate the impedance in the dq reference frame, the grid impedance is filtered out by the PLL below its cut-off frequency as described and observed in [28]. In other words, in the low frequency range, the PLL would also track the perturbation introduced by the PIC (as $G_{\text{GAE}}(s) \rightarrow 1$) and therefore, would introduce an error for the grid impedance estimation as per (4).

So, when tuning the PLL for impedance estimation, there is a trade-off between a large PLL bandwidth frequency (to track fast frequency changes) and small PLL bandwidth frequency (to track the impedance up to low frequencies). This can be well seen in Fig. 2 where, as the t_{set} increases, the PLL minimum frequency $f_{\text{min,PLL}}$ decreases. In this paper, the minimum frequency f_{min} is defined as the frequency point beyond which the magnitude is estimated with a $\pm 50\%$ accuracy.

Considering the injection of a perturbation with zero grid currents (no load steady-state conditions: $I_{\text{d},0} = 0, I_{\text{q},0} = 0$), according to (4) the grid impedance $Z_{\text{qq}}^{\text{est}}(s)$ would be:

$$Z_{\text{qq}}^{\text{est}}(s) = (1 - G_{\text{PLL}}(s)) \cdot Z_{\text{qq}}(s) \quad (6)$$

So, in such conditions, the impedance estimation minimum frequency (beyond which the impedance is correctly estimated with a $\pm 50\%$ accuracy) is equal to the transfer function PLL minimum frequency $f_{\text{min,PLL}}$.
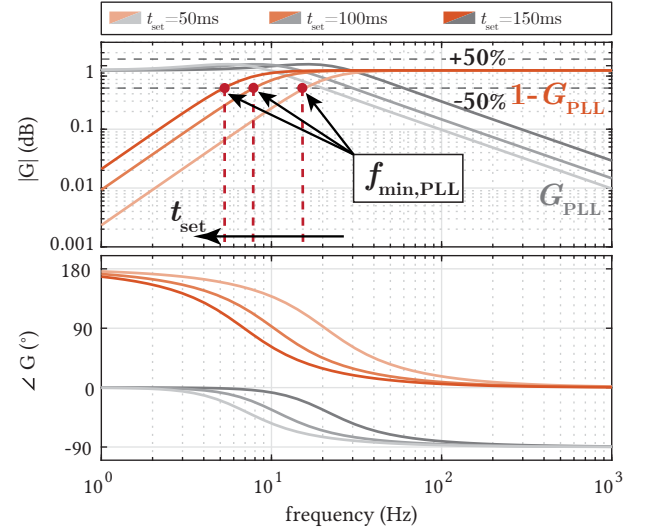
III. IPDFT-BASED GRID ANGLE ESTIMATION

The proposed GAE aims at solving some of the PLL bandwidth limitations for impedance estimation: its high bandwidth frequency value and the dependency on multiple parameters (ξ, t_{set} for a simple PLL). In this paper we propose the use of the IpDFT method, developed for PMUs [30], [31] but never used before for grid impedance estimation. The working principle of the proposed approach is described hereafter.

A. Principle of the method

In Fig. 3, the procedure for the IpDFT-based grid angle estimator is presented. It is based on a three step procedure. Firstly, the grid voltage and current measurements are windowed. Then, an FFT is extracting the frequency components and based on those, an interpolated IpDFT technique determines the grid frequency and the voltage and current phasors. Finally, the positive sequence phasor is extracted and used to compute the grid angle.

1) Windowing: To track precisely the grid frequency, the grid voltages are windowed around a small, moving, window of a few fundamental grid periods (2 to 10), with an update time T_{UP} of typically 1 ms. This allows to track the grid fundamental frequency f_{g} and voltage and current magnitudes $I_{\text{g,abc}}$ and $V_{\text{g,abc}}$ precisely over the whole perturbation injection time (here 8 s).

A Hann windowing [38] is applied to the sampled $V_{\text{g,abc}}$ and $I_{\text{g,abc}}$ to minimize the spectral leakage. Indeed, as seen in Fig. 4, the spectral energy of a pure sinusoid is more concentrated when a Hann window is applied than when a simple rectangular window is applied. Other windows can be used offering similar performance [39], [40]. An FFT is then applied to the windowed data around the grid frequency. Assuming that we are in a grid with known nominal grid frequency $f_{0,\text{nom}}$ and with a maximum recordable time, or
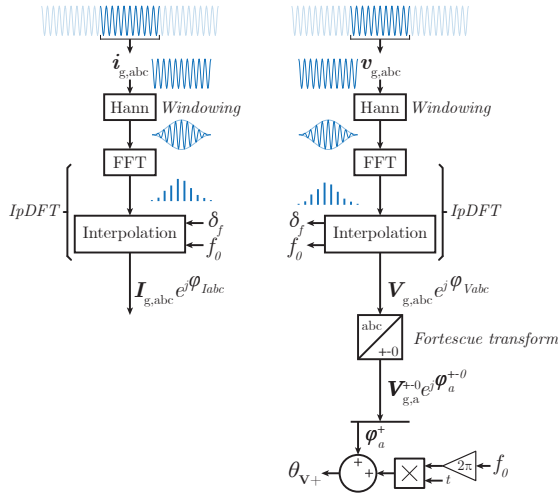
Fig. 3. Procedure for the IpDFT-based grid angle estimator: 1) the grid voltages are used to determine the grid voltage phasors and the grid frequency and 2) the grid frequency is then used to determine the grid current phasors, 3) the voltage phasor positive sequence is extracted to compute the grid angle.
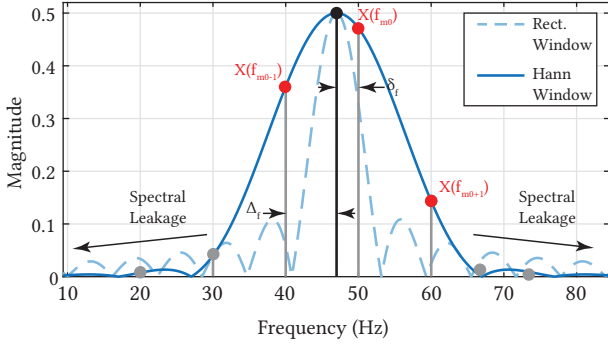

Fig. 4. Example of a frequency waveform of a pure 47Hz sinusoid with a Hann window and a rectangular window.

window time, T_W of 8 s, the frequency step between two bins Δ_f would be:

$$\Delta_\mathrm{f} = \frac{1}{T_\mathrm{W}} \rightarrow \Delta_{\mathrm{f,MAX}} = \frac{1}{8} = 0.125 \text{ Hz} \qquad (7)$$

This precision is far below the potential variations of a conventional grid, where f_g would vary typically by tens of mHz at most. Furthermore, error on the grid angle estimation can lead to improper impedance estimation. To determine precisely the grid frequency, an interpolation technique can be employed to determine the grid frequency in between two bins.

2) Interpolated DFT: IpDFT techniques have been developed by power system researchers and engineers [30], [31] for increasing the precision of the phasor identification of the grid PMUs.

The grid voltages are mainly sinusoids and small signal perturbations should not affect the overall grid voltage sinusoidal shape. As seen in Fig. 4, the DFT of a Hann-windowed sinusoid follows a certain curve. This curve is described as:

$$X(k) = X((f - f_0) \cdot T_\mathrm{W}) = \frac{1}{2} \cdot \frac{\mathrm{sinc}(k)}{1 - k^2} \qquad (8)$$

where k is the kth bin of the DFT.

Therefore, based on the two highest bins (here $X(f_\mathrm{m0})$ and $X(f_{\mathrm{m0}\pm1})$), by using the curve formula, it is possible to determine the fundamental frequency of a grid voltage V_g of unknown frequency [30], [31]:

$$\begin{cases} f_{\mathrm{g},i} & = (m0 + \delta_{\mathrm{f},i}^{\mathrm{est}}) \cdot \Delta f \\ \delta_{\mathrm{f},i}^{\mathrm{est}} & = \epsilon \cdot \frac{2|V_{\mathrm{g},i}(m0+\epsilon)| - |V_{\mathrm{g},i}(m0)|}{|V_{\mathrm{g},i}(m0+\epsilon)| + |V_{\mathrm{g},i}(m0)|} \end{cases} \text{ for } i = \{a,b,c\} \qquad (9)$$

$$\text{where } \epsilon = \begin{cases} +1 \text{ if } |V_{\mathrm{g},i}(m0+1)| > |V_{\mathrm{g},i}(m0-1)| \\ -1 \text{ if } |V_{\mathrm{g},i}(m0+1)| < |V_{\mathrm{g},i}(m0-1)| \end{cases}$$

The frequency deviation is then averaged over the three phases a, b and c to increase the precision:

$$\Delta_\mathrm{f}^{\mathrm{est}} = \frac{\delta_{\mathrm{f,a}}^{\mathrm{est}} + \delta_{\mathrm{f,b}}^{\mathrm{est}} + \delta_{\mathrm{f,c}}^{\mathrm{est}}}{3} \qquad (10)$$

and the estimated phasor $V_{\mathrm{g},i}^{\mathrm{est}} e^{j\angle V_{\mathrm{g},i}^{\mathrm{est}}}$ is:

$$\begin{cases} |V_{\mathrm{g},i}^{\mathrm{est}}| & = |V_{\mathrm{g},i}(m0)| \cdot \left| \frac{\pi\Delta_\mathrm{f}^{\mathrm{est}}}{\sin(\pi\Delta_\mathrm{f}^{\mathrm{est}})} \right| \cdot \left| (\Delta_\mathrm{f}^{\mathrm{est}})^2 - 1 \right| \\ \angle V_{\mathrm{g},i}^{\mathrm{est}} & = \angle V_{\mathrm{g},i}(m0) - \pi \cdot \Delta_\mathrm{f}^{\mathrm{est}} \end{cases} \qquad (11)$$

3) Phasor Computation: As the phasors and the frequency are computed, the grid angle can be computed, based on the positive sequence phase a angle Φ_a^+. The Fortescue transform is applied to the grid voltage phasor $V_{\mathrm{g,abc}} e^{j\Phi_{\mathrm{g,abc}}}$ to obtain the phasor decomposition in the positive, negative and zero sequences:

$$\boldsymbol{V}_{\mathrm{g},+-0} e^{j\angle V_{\mathrm{g},+-0}} = \frac{1}{3} \cdot \begin{bmatrix} 1 & \alpha & \alpha^2 \\ 1 & \alpha^2 & \alpha \\ 1 & 1 & 1 \end{bmatrix} \cdot \boldsymbol{V}_{\mathrm{g,abc}} e^{j\angle V_{\mathrm{g,abc}}} \qquad (12)$$

with $\alpha = e^{j\frac{2\pi}{3}}$

And the grid angle then becomes:

$$\theta_\mathrm{V}^+ = 2\pi f_0 t + \angle V_{\mathrm{g,a+}} \qquad (13)$$

The reason for using the phasor decomposition is not to extract the positive sequence (as we assume a balanced three phase system) but instead to minimize the phase estimation error. In a balanced three phase system, the positive sequence phase $\angle V_{\mathrm{g,a+}}$ is equal to the phase of the grid voltage a $\angle V_{\mathrm{g,a}}$. However, as we have computed the phase for the three phases, we can reduce the grid phase estimated error by utilizing the three grid angle phases, as:

$$\angle V_{\mathrm{g,a}}^{+,\mathrm{est}} = \angle V_{\mathrm{g,a}}^{\mathrm{est}} + \left(\angle V_{\mathrm{g,b}}^{\mathrm{est}} + \frac{2\pi}{3} \right) + \left(\angle V_{\mathrm{g,c}}^{\mathrm{est}} - \frac{2\pi}{3} \right) \qquad (14)$$

B. Parameters Selection

So, when the IpDFT is employed to estimate the grid angle, only three parameters have to be tuned: the window size T_W, the sampling frequency f_S and the update time T_UP. To select the parameter values, a perturbation is injected in the q axis grid voltage and the grid angle is estimated with the proposed method. The perturbation is a single tone, low frequency (5 Hz), low magnitude (10 V) signal and the perturbation is injection during 0.95 s between the time 0.5 s and 4.45 s. The parameters selection must ensure reliable grid angle estimation tracking, meaning maintaining V_q close to 0 V.
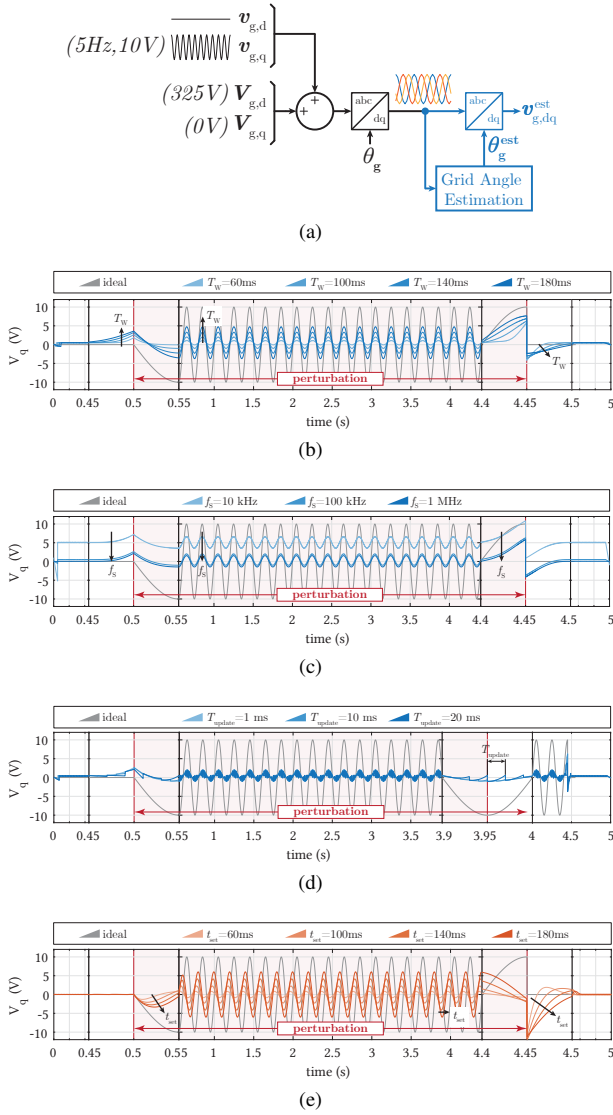
(a)

(b)

(c)

(d)

(e)

Fig. 5. V_q estimation using the IpDFT-based GAE technique during a 4.55 s perturbation (low frequency, low magnitude single tone signal): (a) , (b) windowing time selection, (c) sampling frequency selection, (d) update time selection. (e) Comparison with a PLL-based GAE estimation for different settling times t_{set}.

(a)

(b)

(c)

(d)

Fig. 6. Beginning and ending times of a V_q estimated during a single tone perturbation in the grid voltage q axis for different phase angles using (a),(b) the IpDFT and (c),(d) the PLL techniques to estimate the grid angle.

selected small enough to reduce the initial and final overshoots while ensuring a large enough V_q magnitude for the desired frequency range of interest. In this example, a 100 ms time window is selected.

This initial and final overshoot is dependent on two parameters: the initial and final perturbation phase and the window time width (or equivalently the settling time for the PLL). As seen in Fig. 6, a large initial or final phase can result in an overshoot of up to the perturbation signal magnitude in the case of a 90° phase. The length of the overshoot is however dependent solely on the window time. The initial and final overshoot width are $\frac{T_W}{2}$, as witnessed in Fig. 5b.

2) *Sampling frequency selection*: The IpDFT frequency (and phase) estimation error is mainly caused by the interference of the negative image, that is amplifying low frequency bins magnitude. To reduce this effect, larger sampling frequency can be employed. However, higher sampling frequency would increase both the memory requirements and the computational burden for the post-processing, therefore a trade-off must be found. As it can be seen in Fig. 5c, at 100 kHz and 1 MHz sampling

1) *Window time selection*: as seen in Fig. 5b, when the perturbation is injected, a small V_q overshoot is observed. The larger the window time is, the larger and longer this overshoot is. Meanwhile, the larger the window time is, the smaller the V_q magnitude also is. The same is observed in the end of the perturbation injection. This results in a trade-off where the window time must be
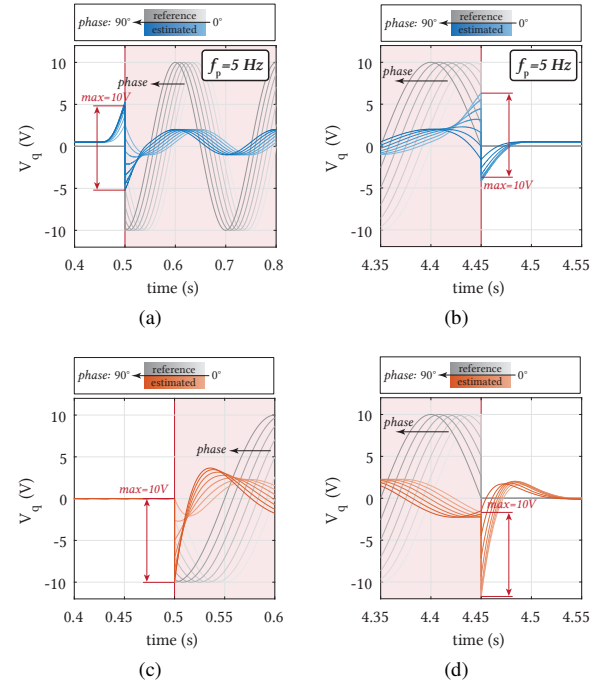
TABLE II
IpDFT PARAMETERS SELECTION VALUES

Steps	T_W	f_S	T_{UP}
1) T_W selection	[60 ms **100 ms** 140 ms 180 ms]	f_S=10 kHz	1 ms
2) f_S selection	**100 ms**	[10 kHz **100 kHz** 1 MHz)]	1 ms
3) T_{UP} selection	**100 ms**	**100 kHz**	[**1 ms** 10 ms 20 ms]

*Note 1: Corresponds to (3 to $9 \cdot T_{0,nom}$)
Note 2: Selected values are in **bold

frequency, the voltage estimation is very close to 0, so a 100 kHz sampling frequency is selected.

3) *Update time selection*: short update time allows for grid frequency and phase corrections at a high frequency. Large update time can reduce the computational burden but at the expense of potentially large errors on the grid angle estimation, caused by the error in the grid frequency. This therefore causes errors in the grid voltage estimation V_q as seen Fig. 5d. An update time of 1 ms is selected as it does not show large V_q ripple or errors, compared to higher values.

All the selected values in this example have been summarized in Table II.

As a comparison, PLL-based grid angle estimation is also performed and it shows similar overshoots at the end of the injection, that decreases in magnitude with the settling time. Compared to the IpDFT-based method, no overshoot is observed in the initial estimation but a certain time is necessary for the V_q to settle at its nominal magnitude. And during operation, the grid voltage also has a delay that is dependent on the the settling time, which is not the case of the IpDFT-based grid angle estimation. An initial comparison of the PLL-based and the IpDFT-based grid angle estimation can already be made:

- At the beginning of the injection, a voltage overshoot is observed prior to the injection time when the IpDFT-based GAE is used.
- During the injection, a voltage dephasing is observed when the PLL is used but not when the IpDFT-based GAE is used.
- At the end of the injection, voltage overshoots are observed for the two grid angle estimation methods but the PLL provokes much larger and longer overshoots (equal to the settling time for the PLL and half the window time for the IpDFT).

C. Transfer function

As seen in Fig. 5b for a single frequency, when an IpDFT-based GAE is used, the voltage $V_{g,q}$ magnitude increases with the window time, however, not phase delay is appearing.

To evaluate the effect of the IpDFT-based GAE on a wide range of frequencies, the process sketched in Fig. 7a is applied, with a wideband perturbation (chirp signal from 1 Hz to 100 Hz) injected in the grid angle, generating a perturbed grid voltage that is then fed to the grid angle estimator. A fast fourier transform is then applied to the angle perturbation $\Delta\theta_g$ and the estimated grid angle perturbation $\Delta\hat{\theta}_g$. The division of the two gives the equivalent transfer function, illustrating the impact of the grid angle estimator on the angle estimation for different frequencies.

The result is drawn in Fig. 7b. As it can be seen, the IpDFT, similar to the PLL acts as a low-pass filter, with very small magnitudes of $1-G_{\text{IpDFT}}$ for low frequencies but a magnitude closer to 1 for higher frequencies (above 20 Hz). The phase is always equal to 0, also observed for 5 Hz in Fig. 5b.
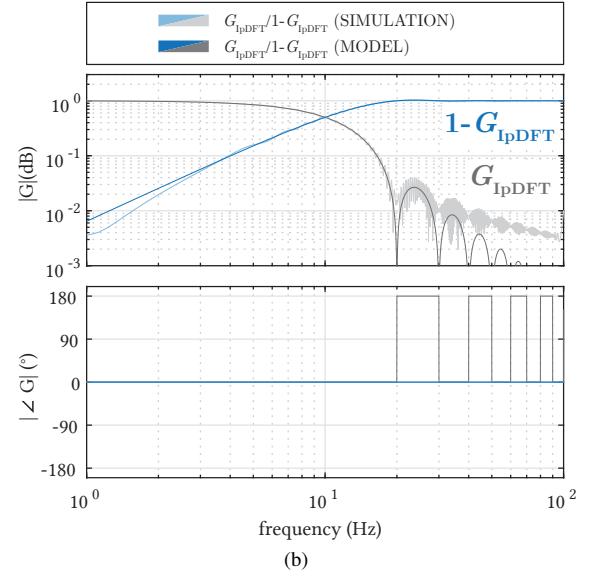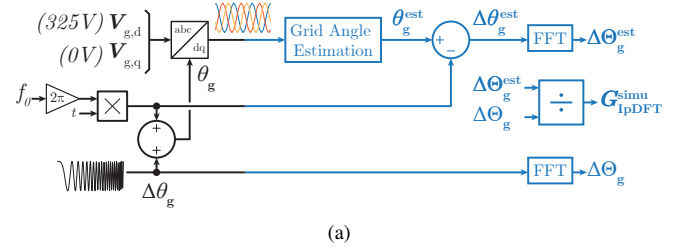

(a)

(b)

Fig. 7. IpDFT-based GAE transfer function (a) estimation process, (b) transfer function model and simulation result comparison.

This transfer function is estimated by the following analytical expression:

$$G_{\text{IpDFT}}^{\text{MODEL}}(s) = \frac{1}{sT_W} \cdot \left(e^{\frac{sT_W}{2}} - e^{-\frac{sT_W}{2}}\right) \cdot \frac{\left(\frac{2\pi}{T_W}\right)^2}{s^2 + \left(\frac{2\pi}{T_W}\right)^2} \quad (15)$$

This transfer function is given by the product of two terms:

- the first term represents the transfer function of an ideal moving average filter over a time window of length T_W (with the window centered between $t - T_W/2$ and $t + T_W/2$), and is responsible for all the antiresonances at the multiple integers of $\frac{1}{T_W}$.
- the second term is a resonance pole that takes into account the non-ideal filtering at the frequency $\frac{1}{T_W}$

As can be noted, there is a good matching between the numerical data and the approximated formula. This transfer function with then be used to compensate the effect of the grid angle estimator, following the same approach as the works of [25], [28] for the PLL.

IV. IMPEDANCE ESTIMATION UNIT

A. Procedure

A conventional method for the impedance measurement [20] shown in Fig. 9, is to inject two orthogonal perturbation signals in the grid line currents (typically in the d axis and then in the q axis) and then measure the perturbed voltages and currents and

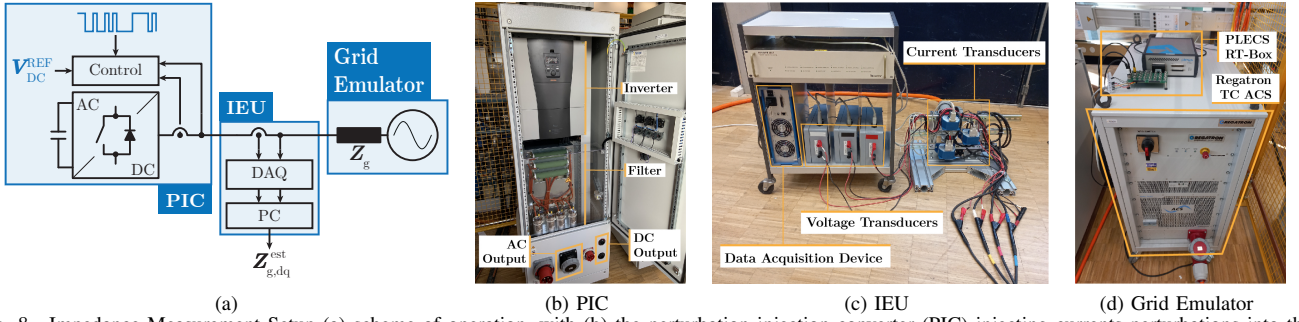| (a)	(b) PIC	(c) IEU	(d) Grid Emulator

Fig. 8. Impedance Measurement Setup (a) scheme of operation, with (b) the perturbation injection converter (PIC) injecting currents perturbations into the grid, (c) an Impedance Estimation Unit (IEU) measuring and recording the currents and voltages and computing the estimated impedance and (d) the grid emulator (Regatron TC ACS) emulating a grid with a given $\boldsymbol{Z}_g$.

estimate the grid impedance. Various perturbation injection signals, sine-sweeps [19], single [17] and multitone signals [41] can be employed. However, when fast impedance estimation is required, pseudo-random binary (PRBS) signals, with rich frequency content, are employed [18], [20]. An additional benefit of using such signal in this study is the concentration of the spectral power density in the low-frequency region [16]. Hence, in this study, a 2 A, 1 kHz PRBS12 (PRBS with a 12 bits shift register [42]) signal is injected in the d and q current references. The grid impedance is estimated in the dq reference frame based on a three step process illustrated in Fig. 9a.

1) The grid angle is estimated with a grid angle estimator.
2) The measured voltages and currents ($\boldsymbol{v}_{\mathrm{g,abc}}$, $\boldsymbol{i}_{\mathrm{g,abc}}$) are transformed in their dq components ($\boldsymbol{v}_{\mathrm{dq}}$, $\boldsymbol{i}_{\mathrm{dq}}$) and the frequency components are extracted. The abc/dq transformation procedure is described in Fig. 9b. The voltages and currents are first transformed in their dq components

(a)

(b)   (c)

Fig. 9. Impedance Measurement Procedure: (a) full procedure, (b) detailed procedure for the abc/dq transformation, (c) detailed procedure for the impedance computation.

using the Clarke-Park transform:

$$\boldsymbol{x}_{\mathrm{dq}} = \boldsymbol{T}_{\mathrm{abc}\to\mathrm{dq}} \cdot \boldsymbol{x}f_{\mathrm{abc}} \tag{16}$$

where

$$\boldsymbol{T}_{\mathrm{abc}\to\mathrm{dq}} = \frac{2}{3} \begin{bmatrix} \cos\left(\theta\right) & \cos\left(\theta - \frac{2\pi}{3}\right) & \cos\left(\theta + \frac{2\pi}{3}\right) \\ -\sin\left(\theta\right) & -\sin\left(\theta - \frac{2\pi}{3}\right) & -\sin\left(\theta + \frac{2\pi}{3}\right) \end{bmatrix} \tag{17}$$

A Fast Fourier Transform (FFT) is then applied to the data.

3) The impedance is estimated using the data for both perturbation signals. Two sequential independent signals [27] are injected as grid current small signal perturbations $\boldsymbol{i}_{\mathrm{g,dq}}^{p}$. By acquiring the voltage response $\boldsymbol{v}_{\mathrm{g,dq}}^{p}$, the grid impedance is then computed as:

$$\boldsymbol{Z}_{\mathrm{g,dq}} = \begin{bmatrix} Z_{\mathrm{g,dd}} & Z_{\mathrm{g,dq}} \\ Z_{\mathrm{g,qd}} & Z_{\mathrm{g,qq}} \end{bmatrix} = \boldsymbol{V}_{\mathrm{g,dq}} \cdot \boldsymbol{I}_{\mathrm{g,dq}}^{-1} \tag{18}$$

where

$$\boldsymbol{V}_{\mathrm{g,dq}}(f) = \begin{bmatrix} v_{\mathrm{g,d}}^{1} & v_{\mathrm{g,d}}^{2} \\ v_{\mathrm{g,q}}^{1} & v_{\mathrm{g,q}}^{2} \end{bmatrix}, \boldsymbol{I}_{\mathrm{g,dq}}(f) = \begin{bmatrix} i_{\mathrm{g,d}}^{1} & i_{\mathrm{g,d}}^{2} \\ i_{\mathrm{g,q}}^{1} & i_{\mathrm{g,q}}^{2} \end{bmatrix} \tag{19}$$

B. Experimental Setup

Results in this paper are all based on experimental data from experiments conducted with the setup pictured in Fig. 8. The setup is composed of three elements: a grid emulator, a perturbation injection converter and an impedance estimation unit at the PCC between the converter and the grid emulator as illustrated in Fig. 8a. The grid emulator, pictured in Fig. 8d, is based on the Regatron TC ACS grid simulator device controlled by a Plexim RT-Box device. Current measurements of the TC.ACS are read by the RT-Box that, according to the desired grid impedance, computes and generates analog voltage references for the TC.ACS device. By having the scheme of a grid with a certain grid impedance $\boldsymbol{Z}_g$ (pure resistance, in-series R+L...) in the RT-Box, it is possible to emulate the grid behaviour with any impedance value (compatible with the bandwidth of the power hardware: the total delay time is around 135 μs so the system can emulate an impedance correctly up to 1.5 kHz ($\frac{1}{5 \cdot T_{\mathrm{W}}}$). The perturbation injection has been integrated on top of an active-front end performing a standard control of the DC voltage and reactive power. The AFE current control bandwidth is around 1 kHz.
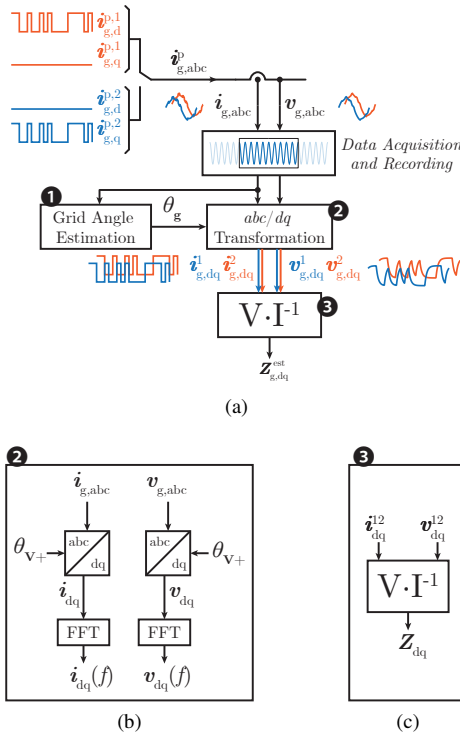
PRBS signals are superimposed to the d and q axes current references (axes are determined by an internal PLL). Fig. 8b presents the PIC internal elements.

The impedance estimation unit, illustrated in Fig. 8c is based on measurements from LEM IT 60-S Ultrastab current transducers and LEM CV 3-1000V 1:100 voltage modules. The acquisition device is a 32 14 bits channels Elsys Tranet 408S. Data is sampled at a sampling rate of 20 MS/s, an averaging is performed using a 100 kHz anti-aliasing filter, leading to an effective sampling frequency of 1 MHz. Memory size allows a maximum recording time of 8 s.

V. IMPEDANCE ESTIMATION USING IPDFT

The IpDFT-based grid angle estimation method presented in Fig. 3 is compared to the offline PLL method presented in the previous section using the standard parameters defined in Table III. To be comparable, the IpDFT and the PLL methods are using the same sampling frequency (100 kHz) and the IpDFT is using a window time equivalent to the PLL settling time (100 ms). A 1 kHz PRBS signal of 2 A magnitude is injected in the grid by the active front end. The methods are then compared for different emulated grid impedances.

A. Frequency and angle tracking for PLL and IpDFT methods

The PLL and IpDFT grid angle estimation tracking performance is presented in this section. As described in Section II, when a perturbation is occuring in the q axis of the voltage,

the grid angle estimation is also being perturbed. To illustrate the equivalent performance of the PLL and IpDFT in their function, the angle tracked by a PLL and by an IpDFT are drawn in Fig. 10. What can be noticed first is the large ripples in the frequency estimation of the PLL (up to 100 mHz) whereas the IpDFT-based technique is much more stable but has a small bias (around 70 mHz). When, at 0.5 s, a 2 V 1 kHz perturbation is injected in the q axis grid voltage, the frequency estimation is visibly disturbed by the perturbation with a grid frequency perturbed up to 20 mHz. However, the resulting perturbation in the grid angle is not very visible, and both the PLL and the IpDFT-based techniques are ensuring good overall grid angle tracking.

To conclude, the PLL and the IpDFT seem to perform their grid angle estimation similarly with some small differences in terms of ripple and oscillation magnitudes. To evaluate the impact of those in the impedance estimation, in the following section, an impedance is estimated using the IpDFT-based technique.

B. Effect of the IpDFT parameters on the impedance estimation

The parameters of the IpDFT modify the response of the grid angle estimator as described in Section III-C and hence impact the impedance estimation. Two IpDFT parameters are to be investigated: T_W, because it acts on the IpDFT response, and f_S, because it affects the time resolution. Since

TABLE III
BASE VALUES FOR THE SYSTEM PARAMETERS

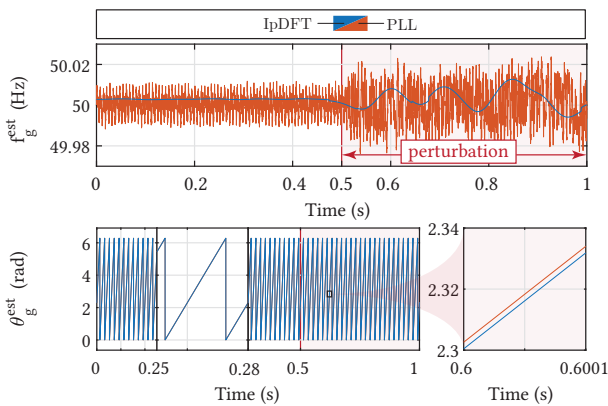| Parameter	Value
f_g	40.90 Hz
V_g	325 V
Z_g	1 Ω
f_S	100 kHz
t_{set}	100 ms
ξ	$\frac{1}{\sqrt{2}}$
T_W	100 ms
T_{UP}	1 ms

Fig. 10. PLL and IpDFT-based grid frequency and angle estimation before and during voltage perturbation (in the q axis).
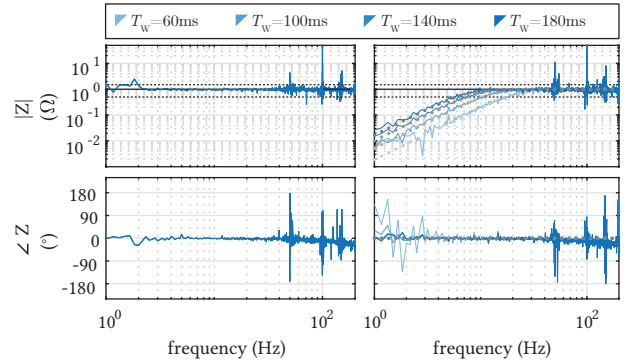

Fig. 11. IpDFT-based impedance estimation for different window sizes T_W, in dotted line: $1 - G_{\text{IpDFT}}^{\text{MODEL}}$.
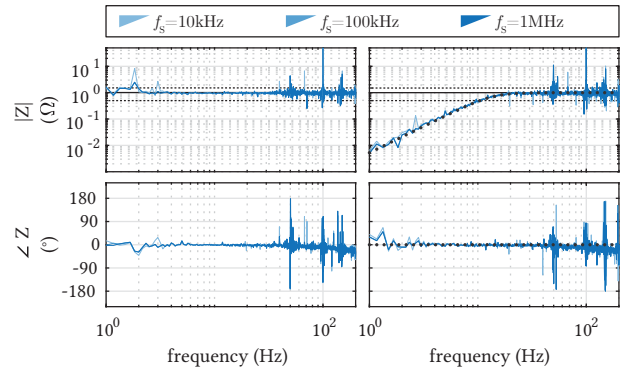

Fig. 12. IpDFT-based impedance estimation for different sampling frequencies f_S, in dotted line: $1 - G_{\text{IpDFT}}^{\text{MODEL}}$.

the grid frequency is stable, the update time does not have any direct impact on the impedance estimation and the value defined in Table II is used (1 ms). To evaluate the impact of the parameters, a purely resistive grid impedance of $1\,\Omega$ is emulated by the grid emulator and a 1 kHz 2 A PRBS signal is injected in the grid.

As observed in Figs. 11 and 12, the grid impedance estimation in Z_{qq} is distorted following the same tendency as the PLL (-20 dB/dec below a minimum frequency f_{min}) for the magnitude but it has no impact on the phase (the PLL, on the other hand, dephases the angle by 90°). This is well predicted by the estimated IpDFT transfer function derived in Section III-C and drawn in the figure. The effect of the sampling frequency is also investigated in Fig. 12 and it can be seen that above 100 kHz, it has a very minor impact in the grid impedance estimation.

C. Grid Angle Estimator Effect Compensation

As the impact of the grid angle estimator on Z_{qq}^{est} can be well predicted and modeled, it can also be compensated following:

$$Z_{qq}^{est,comp}(j\omega) = (1 - G_{GAE}(j\omega))^{-1} \cdot Z_{qq}^{est}(j\omega) \quad (20)$$

The compensated $1\,\Omega$ impedance is compared to the non-compensated impedance in Fig. 13 using both a PLL or a IpDFT as a GAE. The compensation algorithm corrects accurately the impedance for both grid angle estimator techniques with a Z_{qq} now contained around $1\,\Omega$ even at low frequencies. However, one can notice the small ripple at low frequency (1 Hz to 5 Hz). To evaluate this noise, two indicators are used: the maximum magnitude error and the impedance variance. Both of those indicators are evaluated on $|Z_{qq}|$ in
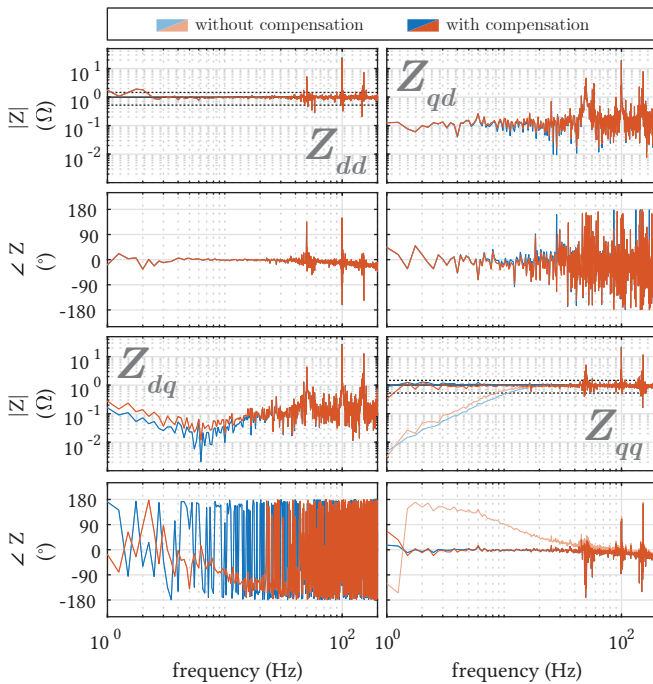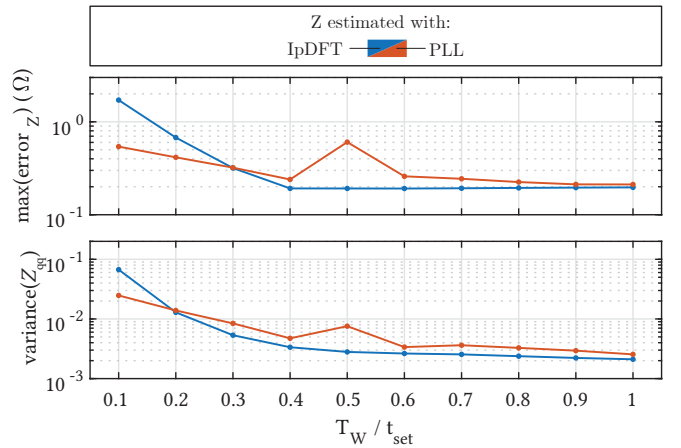

Fig. 14. maximum error and variance on the impedance (from 2 Hz to 100 Hz using a PLL-based grid angle estimator or an IpDFT-based grid angle estimator), $Z_g = R = 1\,\Omega$.

the $[2\,\Omega, 10\,\Omega]$ frequency range for different window times. In Fig. 14, the results for a pure resistive grid impedance of $1\,\Omega$ are plotted. Above 400 mHz, both indicators show better results when the IpDFT-based GAE is used. For instance, using a window time or a settling time of 800 ms, the maximum error on the impedance is of 225 mΩ for the PLL and 194 mΩ for the IpDFT (-13 %) and the impedance variance is of 3.3 mΩ and 2.4 mΩ (-27 %).

To confirm this tendency for the IpDFT-based grid angle estimator to perform better in the low frequency range, the variance indicator is applied to other grid impedances.

D. Performance with Different Grid Impedance

The impedance estimation has been performed on various passive grid impedances, with different low-frequency and high-frequency impedance characteristics. Firstly, different resistance values for a pure resistive grid impedance have been emulated, ranging from $0.5\,\Omega$ to $2\,\Omega$. Resulting impedances are plotted in Fig. 15b for a window time or a settling time of 400 mΩ. The impedance variance has been plotted in Fig. 15a. As it can be seen, similar trends as what has been seen in Fig. 14, with a variance that decreases with the window time and that is generally larger for the PLL than for the IpDFT, beyond 200 ms and 400 ms. Using the IpDFT-based GAE, and compared to the PLL, for the $0.5\,\Omega$ impedance, the estimation is up to 18 % better (for a window time of 400 ms). For the $1\,\Omega$ impedance, the estimation is better by 20 % to 40 % above 300 ms and for the $2\,\Omega$ impedance, the estimation is better by 30 % to 300 %.

A RL impedance is then emulated with the grid emulator and estimated in Fig. 16b. With such impedance, the variance is also much larger (from 130 % and up to 160 %) beyond 300 ms for the PLL-based estimated impedance, when compared to the IpDFT-based one.

Finally, to confirm results when using a grid emulator, a real grid impedance has been used. A LC filter from EPCOS has been inserted between the grid emulator and the impedance estimation unit. In Fig. 17b, the estimated LC filter impedance
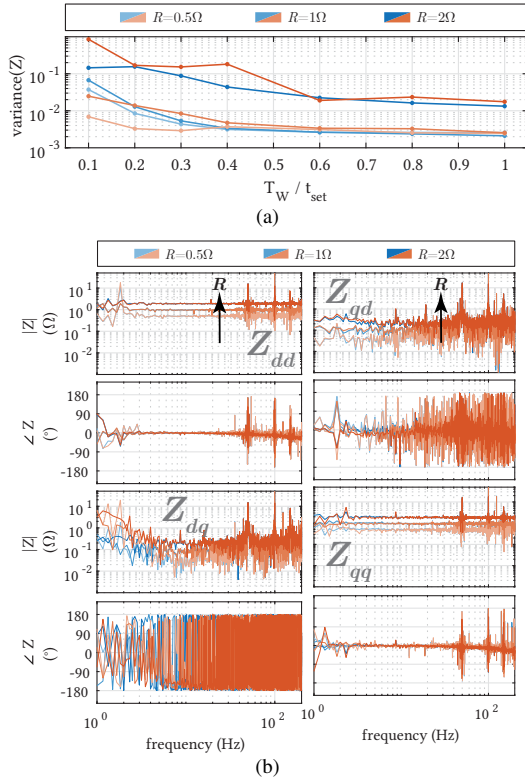

Fig. 13. IpDFT-based and PLL-based impedance estimation without and with compensation, $Z_g = R = 1\,\Omega$.

Fig. 15. PLL-based and IpDFT-based impedance estimation for different impedances $Z_g = R = \{0.5\,\Omega, 1\,\Omega, 2\,\Omega\}$ (a) variance on the impedance, (b) impedance for $T_W/t_{set} = 400\,ms$.
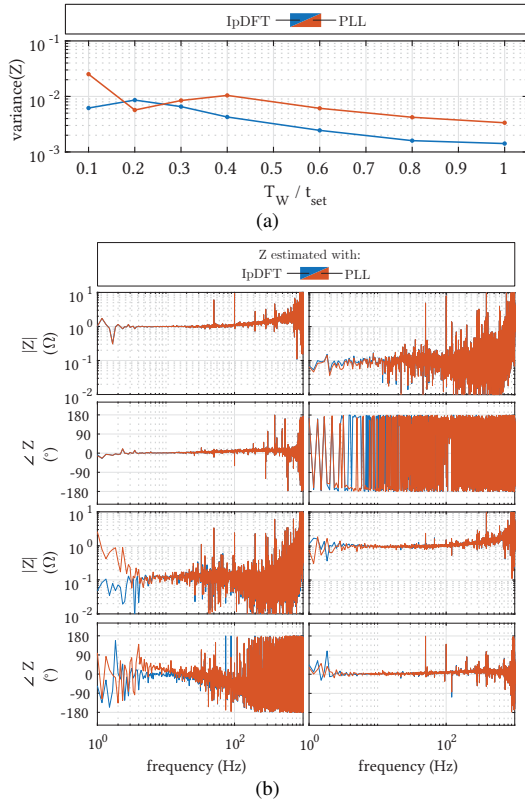

Fig. 16. PLL-based and IpDFT-based impedance estimation for a inductive impedance: $Z_g = R_g + j\omega_g L_g$. $R_g = 1\,\Omega$, $L_g = 300\,\mu H$ (a) variance on the impedance, (b) impedance for $T_W/t_{set} = 400\,ms$.
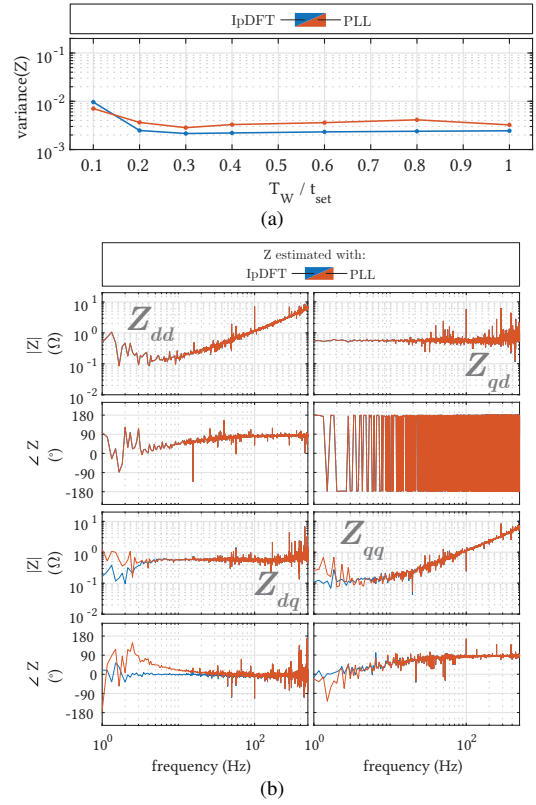

Fig. 17. PLL-based and IpDFT-based impedance estimation of an LC filter (EPCOS B84143V003R127) (a) variance on the impedance, (b) impedance for $T_W/t_{set} = 400\,ms$.

is plotted with a very low impedance at low frequencies (around $100\,m\Omega$). As seen in Fig. 17a, the variance is also larger when the PLL is used compared to when the IpDFT-based GAE is used. Using the IpDFT as a grid angle estimatro, the variance on the impedance is reduced by 32 % to 72 %.

Those results, using different impedances with different low frequency impedance values (ranging from $100\,m\Omega$ to $2\,\Omega$), confirm that the IpDFT-based method shows better results in the low frequency range compared to the conventional PLL-based method.

VI. CONCLUSION

Self-synchronizing impedance measurement (grid frequency is tracked based on the acquired grid voltages) in the dq frame is unreliable at low frequencies due to the effect of the grid angle estimator, that causes a distortion and large noise in the Z_{qq} at low frequency, depending on its bandwidth. A trade-off between a fast grid angle tracking and good impedance estimation must therefore be found.

Conventionally, a PLL is used to track the grid angle, however, the impedance quality at low frequencies is not very good with relatively large noise levels, indicated by a large impedance variance.

The grid angle estimator proposed in this paper is using an IpDFT technique, which computes the grid frequency based on an interpolation of bins of a Fourier transform around the fundamental frequency. This method shows similar transfer function properties as the PLL and can hence similarly

be compensated. However, the resulting impedance shows a higher quality in the estimation, with lower variances, for all types of impedances estimated and different low-frequency impedance values. This method can thus serve as a good grid angle estimator for impedance estimation.

REFERENCES

[1] J. Wang, C. Jin, and P. Wang, "A Uniform Control Strategy for the Interlinking Converter in Hierarchical Controlled Hybrid AC/DC Microgrids," *IEEE Transactions on Industrial Electronics*, vol. 65, no. 8, pp. 6188–6197, Aug. 2018.

[2] G. Melath, S. Rangarajan, and V. Agarwal, "A Novel Control Scheme for Enhancing the Transient Performance of an Islanded Hybrid AC–DC Microgrid," *IEEE Transactions on Power Electronics*, vol. 34, no. 10, pp. 9644–9654, Oct. 2019.

[3] J. Enslin and P. Heskes, "Harmonic interaction between a large number of distributed power inverters and the distribution network," *IEEE Transactions on Power Electronics*, vol. 19, no. 6, pp. 1586–1593, Nov. 2004.

[4] D. Bazargan, S. Filizadeh, and A. M. Gole, "Stability Analysis of Converter-Connected Battery Energy Storage Systems in the Grid," *IEEE Transactions on Sustainable Energy*, vol. 5, no. 4, pp. 1204–1212, Oct. 2014.

[5] T. Messo, J. Jokipii, A. Aapro, and T. Suntio, "Time and frequency-domain evidence on power quality issues caused by grid-connected three-phase photovoltaic inverters," in *2014 16th European Conference on Power Electronics and Applications*, Aug. 2014, pp. 1–9.

[6] E. Mollerstedt and B. Bernhardsson, "Out of control because of harmonics-an analysis of the harmonic response of an inverter loco-motive," *IEEE Control Systems Magazine*, vol. 20, no. 4, pp. 70–81, Aug. 2000.

[7] C. Buchhagen, C. Rauscher, A. Menze, and J. Jung, "BorWin1 - First Experiences with harmonic interactions in converter dominated grids," in *International ETG Congress 2015; Die Energiewende - Blueprints for the new energy age*, Nov. 2015, pp. 1–7.

[8] H. Saad, Y. Fillion, S. Deschanvres, Y. Vernay, and S. Dennetière, "On Resonances and Harmonics in HVDC-MMC Station Connected to AC Grid," *IEEE Transactions on Power Delivery*, vol. 32, no. 3, pp. 1565–1573, Jun. 2017.

[9] H. Saad, A. Schwob, and Y. Vernay, "Study of Resonance Issues Between HVDC Link and Power System Components Using EMT Simulations," in *2018 Power Systems Computation Conference (PSCC)*, Jun. 2018, pp. 1–8.

[10] R. D. Middlebrook and S. Cuk, "A general unified approach to modelling switching-converter power stages," in *1976 IEEE Power Electronics Specialists Conference*, Jun. 1976, pp. 18–34.

[11] M. Belkhayat, *Stability criteria for AC power systems with regulated loads*. Purdue University, 1997.

[12] Z. Yao, P. Therond, and B. Davat, "Stability analysis of power systems by the generalised nyquist criterion," in *1994 International Conference on Control-Control'94.*, vol. 1. IET, 1994, pp. 739–744.

[13] B. Wen, D. Boroyevich, R. Burgos, P. Mattavelli, and Z. Shen, "Small-Signal Stability Analysis of Three-Phase AC Systems in the Presence of Constant Power Loads Based on Measured d-q Frame Impedances," *IEEE Transactions on Power Electronics*, vol. 30, no. 10, pp. 5952–5963, Oct. 2015.

[14] T. Messo, A. Aapro, and T. Suntio, "Generalized multivariable small-signal model of three-phase grid-connected inverter in DQ-domain," in *2015 IEEE 16th Workshop on Control and Modeling for Power Electronics (COMPEL)*, Jul. 2015, pp. 1–8.

[15] G. Francis, R. Burgos, D. Boroyevich, F. Wang, and K. Karimi, "An algorithm and implementation system for measuring impedance in the D-Q domain," in *2011 IEEE Energy Conversion Congress and Exposition*, Sep. 2011, pp. 3221–3228.

[16] H. Gong, X. Wang, and D. Yang, "DQ-Frame Impedance Measurement of Three-Phase Converters Using Time-Domain MIMO Parametric Iden-tification," *IEEE Transactions on Power Electronics*, vol. 36, no. 2, pp. 2131–2142, Feb. 2021.

[17] L. Asiminoaei, R. Teodorescu, F. Blaabjerg, and U. Borup, "A digital controlled PV-inverter with grid impedance estimation for ENS detec-tion," *IEEE Transactions on Power Electronics*, vol. 20, no. 6, pp. 1480–1490, Nov. 2005.

[18] T. Roinila, T. Messo, and E. Santi, "MIMO-Identification Techniques for Rapid Impedance-Based Stability Assessment of Three-Phase Systems in DQ Domain," *IEEE Transactions on Power Electronics*, vol. 33, no. 5, pp. 4015–4022, May 2018.

[19] Z. Shen, M. Jaksic, P. Mattavelli, D. Boroyevich, J. Verhulst, and M. Belkhayat, "Three-phase AC system impedance measurement unit (IMU) using chirp signal injection," in *2013 Twenty-Eighth Annual IEEE Applied Power Electronics Conference and Exposition (APEC)*, Mar. 2013, pp. 2666–2673.

[20] A. Riccobono, M. Mirz, and A. Monti, "Noninvasive Online Parametric Identification of Three-Phase AC Power Impedances to Assess the Stability of Grid-Tied Power Electronic Inverters in LV Networks," *IEEE Journal of Emerging and Selected Topics in Power Electronics*, vol. 6, no. 2, pp. 629–647, Jun. 2018.

[21] A. Knop and F. W. Fuchs, "High frequency grid impedance analysis by current injection," in *2009 35th Annual Conference of IEEE Industrial Electronics*, Nov. 2009, pp. 536–541.

[22] D. Martin, I. Nam, J. Siegers, and E. Santi, "Wide bandwidth three-phase impedance identification using existing power electronics inverter," in *2013 Twenty-Eighth Annual IEEE Applied Power Electronics Conference and Exposition (APEC)*, Mar. 2013, pp. 334–341.

[23] M. O. Prates, C. A. Duque, P. G. Barbosa, A. S. Cerqueira, A. Testa, and P. F. Ribeiro, "Power system impedance measurement based on wavelet voltage imposed," in *2014 16th International Conference on Harmonics and Quality of Power (ICHQP)*, May 2014, pp. 798–802.

[24] A. Riccobono, E. Liegmann, A. Monti, F. Castelli Dezza, J. Siegers, and E. Santi, "Online wideband identification of three-phase AC power grid impedances using an existing grid-tied power electronic inverter," in *2016 IEEE 17th Workshop on Control and Modeling for Power Electronics (COMPEL)*, Jun. 2016, pp. 1–8.

[25] Z. Shen, M. Jaksic, B. Zhou, P. Mattavelli, D. Boroyevich, J. Verhulst, and M. Belkhayat, "Analysis of Phase Locked Loop (PLL) influence on DQ impedance measurement in three-phase AC systems," in *2013 Twenty-Eighth Annual IEEE Applied Power Electronics Conference and Exposition (APEC)*, Mar. 2013, pp. 939–945.

[26] J. Jokipii, T. Messo, and T. Suntio, "Simple method for measuring output impedance of a three-phase inverter in dq-domain," in *2014 International Power Electronics Conference (IPEC-Hiroshima 2014 - ECCE ASIA)*, May 2014, pp. 1466–1470.

[27] M. Berg, H. Alenius, and T. Roinila, "Rapid Multivariable Identification of Grid Impedance in DQ Domain Considering Impedance Coupling," *IEEE Journal of Emerging and Selected Topics in Power Electronics*, vol. 10, no. 3, pp. 2710–2721, Jun. 2022.

[28] H. Gong, D. Yang, and X. Wang, "Impact of Synchronization Phase Dy-namics on DQ Impedance Measurement," in *2018 IEEE 19th Workshop on Control and Modeling for Power Electronics (COMPEL)*, Jun. 2018, pp. 1–7.

[29] W. Zhou, Y. Wang, R. E. Torres-Olguin, and Z. Chen, "Frequency Scanning-Based Contributions Identification of Current Control Loop and PLL on DQ Impedance Characteristics of Three-Phase Grid-Connected Inverter," in *2020 IEEE Energy Conversion Congress and Exposition (ECCE)*, Oct. 2020, pp. 3104–3111.

[30] D. C. Rife and G. A. Vincent, "Use of the discrete fourier transform in the measurement of frequencies and levels of tones," *The Bell System Technical Journal*, vol. 49, no. 2, pp. 197–228, Feb. 1970.

[31] C. Offelli and D. Petri, "The influence of windowing on the accuracy of multifrequency signal parameter estimation," *IEEE Transactions on Instrumentation and Measurement*, vol. 41, no. 2, pp. 256–261, Apr. 1992.

[32] H. Zhou, X. Zhao, D. Shi, H. Zhao, and C. Jing, "Calculating sequence impedances of transmission line using PMU measurements," in *2015 IEEE Power & Energy Society General Meeting*, Jul. 2015, pp. 1–5.

[33] P. A. Pegoraro, K. Brady, P. Castello, C. Muscas, and A. von Meier, "Line Impedance Estimation Based on Synchrophasor Measurements for Power Distribution Systems," *IEEE Transactions on Instrumentation and Measurement*, vol. 68, no. 4, pp. 1002–1013, Apr. 2019.

[34] R. Puddu, K. Brady, C. Muscas, P. A. Pegoraro, and A. Von Meier, "PMU-Based Technique for the Estimation of Line Parameters in Three-Phase Electric Distribution Grids," in *2018 IEEE 9th International*

Workshop on Applied Measurements for Power Systems (AMPS), Sep. 2018, pp. 1–5.

[35] B. Alinezhad and H. Kazemi Karegar, "On-Line Thévenin Impedance Estimation Based on PMU Data and Phase Drift Correction," *IEEE Transactions on Smart Grid*, vol. 9, no. 2, pp. 1033–1042, Mar. 2018.

[36] K. Moffat, M. Bariya, and A. Von Meier, "Real Time Effective Impedance Estimation for Power System State Estimation," in *2020 IEEE Power & Energy Society Innovative Smart Grid Technologies Conference (ISGT)*, Feb. 2020, pp. 1–5.

[37] R. Teodorescu, M. Liserre, and P. Rodriguez, *Grid Converters for Photovoltaic and Wind Power Systems*, 1st ed. John Wiley & Sons, Ltd, 2010.

[38] *Advances in Power System Modelling, Control and Stability Analysis*. IET Digital Library, Sep. 2016.

[39] F. Harris, "On the use of windows for harmonic analysis with the discrete Fourier transform," *Proceedings of the IEEE*, vol. 66, no. 1, pp. 51–83, Jan. 1978.

[40] A. Derviškadić, P. Romano, and M. Paolone, "Iterative-interpolated DFT for synchrophasor estimation in M-class compliant PMUs," in *2017 IEEE Manchester PowerTech*, Jun. 2017, pp. 1–6.

[41] M. Jaksic, Z. Shen, I. Cvetkovic, D. Boroyevich, R. Burgos, and P. Mattavelli, "Wide-bandwidth Identification of small-signal dq impedances of ac power systems via single-phase series voltage injection," in *2015 17th European Conference on Power Electronics and Applications (EPE'15 ECCE-Europe)*, Sep. 2015, pp. 1–10.

[42] L. Ljung, *System Identification: Theory for the User*, 2nd ed. Upper Saddle River, NJ: Pearson, Dec. 1998.

Jules Mace received the B.S. and M.Sc. degree in electrical engineering from the National Institute of Applied Sciences (INSA) of Toulouse, France in 2020, and the M.Sc. degree from the Seoul National University, South Korea, in 2020. He is, since 2020, a PhD student with the Power Electronics Laboratory, École Polytechnique Fédérale de Lausanne, Switzerland. His research interests include power converter modeling and design, system identification and stability in hybrid AC/DC power distribution networks.

Andrea Cervone received the B.Sc., M.Sc., and Ph.D. degrees in electrical engineering from the University of Naples Federico II, Naples, Italy, in 2014, 2017, and 2021, respectively. He is currently a post-doc at the Power Electronics Laboratory of the École Polytechnique Fédérale de Lausanne (EPFL). His research interests include modeling and control of power electronics converters and electrical drives.

Drazen Dujic received the Dipl.Ing. and M.Sc. degrees in electrical engineering from the University of Novi Sad, Novi Sad, Serbia, in 2002 and 2005, respectively, and the Ph.D. degree in electrical engineering from Liverpool John Moores University, Liverpool, U.K., in 2008. From 2002 to 2006, he was with the Department of Electrical Engineering, University of Novi Sad as a Research Assistant. From 2006 to 2009, he was with Liverpool John Moores University as a Research Associate. From 2009 to 2013, he was with the ABB Corporate Research Centre, Switzerland, as the Principal Scientist working on the power electronics projects spanning the range from low-voltage/power SMPS in below kilowatt range to medium voltage high-power converters in a megawatt range. From 2010 to 2011, he was a Member of a project team responsible for the development of the world's first power electronic traction transformer successfully commissioned on the locomotive. From 2013 to 2014, he was with ABB Medium Voltage Drives, Turgi, Switzerland, as a Research and Development Platform Manager responsible for ABB's largest IGCT-based medium voltage drive ACS6000.

He is currently with the École Polytechnique Fédérale de Lausanne, Lausanne, Switzerland, as an Associate Professor and the Director of the Power Electronics Laboratory. He has authored or coauthored more than 200 scientific publications and has filed 18 patents. His current research interests include the areas of design and control of advanced high-power electronics systems for medium voltage applications.

Dr. Dujic has received the First Prize Paper Award from the Electric Machines Committee of the IEEE Industrial Electronics Society, in 2007, the Isao Takahashi Power Electronics Award for Outstanding Achievement in Power Electronics in 2014, and the EPE Outstanding Service Award from the European Power Electronics and Drives Association in 2018. He is an Associate Editor of the IEEE TRANSACTIONS ON POWER ELECTRONICS.